MATEC Web of Conferences **146**, 02004 (2018) https://doi.org/10.1051/matecconf/201814602004
*Building Defects 2017*

# Comparison of engineered cementitious composites and concrete for strengthening of concrete structural details using RBSM

*Yuliia* Khmurovska[1] , and *Petr* Štemberk[1,*]

[1]Czech Technical University, Thákurova 7, 166 29 Prague 6, Czech Republic

**Abstract.** This paper presents a numerical simulation and subsequent comparison of strengthening performance of an ordinary concrete overlay and an overlay made of engineered cementitious composite (ECC) with polyvinyl alcohol fibers (PVA). The comparison is performed on an L-shaped joint when the overlay is placed on the outer surface so that the applied bending moment causes tension in the overlay. The nonlinear numerical analysis is based on the three-dimensional rigid-body-spring model (RBSM). The results show the beneficial effect of the PVA fibers within the ECC matrix when the damage is distributed evenly so that only thin microcracks open. The observation is easy to obtain when the RBSM is employed. On the contrary, the overlay made of ordinary concrete fails due to localization of the damage into a single crack. The applicability of the RBSM is discussed.

## 1 Introduction

Durability, which is one of the basic requirements for concrete structures, is to a large extent ensured by a cover layer. Since the cover layer of concrete is subjected to direct exposure to aggressive environment, its degradation is a frequent cause of structural repair. Carbonization can be taken as the typical example of concrete cover degradation (Figure 1), which can be divided into 3 stages. Firstly, the cover layer is damaged by the imperfection of material and volumetric changes that are caused by shrinkage, temperature difference etc. Secondly, the concrete cover layer loses its protective properties so much that the reinforcement begins to corrode, which causes further cracking of concrete. Thirdly, rebars corrode up to the load bearing limit and destruction of cover layer [1]. Due to this process, the damaged part of concrete has to be removed and replaced with suitable material.

In this work, the engineered cementitious composite (ECC) is considered as an alternative repair material. 2% by volume of polyvinyl alcohol fibers (PVA), [3], are added to the mixture to reduce shrinkage effect and to increase adhesion properties of ECC. The main advantage of PVA-ECC is its tensile strain capacity in the range of 3-7% [4], and strain hardening behavior that is achieved by cement matrix multiple cracking [5]. The performance of PVA-ECC in tension is characterized by appearance of large number of

* Corresponding author: stemberk@fsv.cvut.cz

microcracks that provide slower transport of environmental products as compared with ordinary concrete, where the crack localization take place from the very beginning.

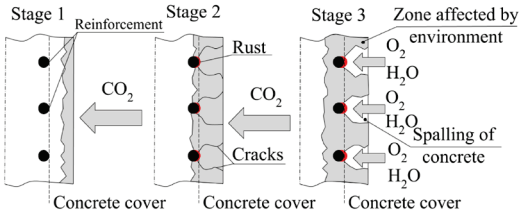


**Fig. 1.** Deterioration of reinforced concrete [1].

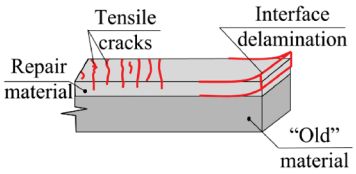


**Fig. 2.** Cover layer failure modes [2].

The repair material layer of structural elements subjected to bending has to withstand tensile stresses that develop in a tensile part of bended structure and shear stresses that appear along the interface between "old" and "new" materials [2]. Tensile stresses may provoke the repair material cracking, while shear stresses may be a cause of repair layer delamination. Possible failure modes of repair system are shown in Figure 2.

3D Rigid-Body-Spring Model (RBSM) is used to perform the numerical simulation in this work in order to analyze both the crack patterns and the repair layer delamination.

## 2 Material model

The Rigid-Body-Spring Model (RBSM) is a type of a discrete method model which was invented by Kawai [6]. The main benefit of the RBSM is its relatively simple constitute formulation that can be validated easily by classical benchmark tests. The random geometry of the particles provided by Voronoi tessellation [7], helps to simulate crack patterns and their propagation and to reduce mesh bias. The material is modeled as a set of undeformable rigid bodies interconnected by sets of springs on their surfaces. In the presented model, each rigid body has six degrees of freedom (3 translational and 3 rotational) defined at the nuclei of the Voronoi cells. In the modified formulation of RBSM, each split triangular surface consists of a set of one normal and two shear springs, which account for the effect of bending and torsion without the use of rotational springs [8].

### 2.1 Concrete material model

The material model within the 3D RBSM for the concrete substrate (original concrete part of the structure) in tension, compression and shear is defined in Figure 3 for easy understanding. All material parameters used later in the analyses are provided below. The tensile stress-strain relation for the normal springs is linear elastic with the slope corresponding to the elastic modulus, $E$, up to tensile-strength dependent value $\sigma_t$ with the bilinear softening behavior after cracking as shown in Figure 3a) [8, 9]. In Figure 3a), $f_t$ is the tensile strength, $E_{exp}$ is the experimentally obtained elastic modulus, $G_f$ is the fracture energy and $h$ is the distance between the nuclei of the neighboring rigid-bodies. The compression model for the normal springs is modeled as a combination of two quadratic functions with the resultant S-shape curve (Figure 3b)). In Figure 3 b), $f_c$ is the compressive strength. The model considers only the failure in tension or shear, as compressive failure does not occur [8, 9]. The compression model is given by the following formulas

$$\sigma = \begin{cases} a_0\varepsilon^2 + b_0\varepsilon & \varepsilon > \varepsilon_{c1} \\ a_1\varepsilon^2 + b_1\varepsilon + c_1 & \varepsilon \le \varepsilon_{c1} \end{cases} \quad (1)$$

where $a_0 = -\dfrac{E(1-\alpha_{c1})}{2\varepsilon_{c1}}$, $b_0 = E$, $a_1 = -\dfrac{E(\alpha_{c2}-\alpha_{c1})}{2(\varepsilon_{c2}-\varepsilon_{c1})}$, $b_1 = -\dfrac{E(\alpha_{c1}\varepsilon_{c2}-\alpha_{c2}\varepsilon_{c1})}{\varepsilon_{c2}-\varepsilon_{c1}}$,

$c_1 = -a_1\varepsilon_{c1}^2 + b_1\varepsilon_{c1} + \sigma_c$.

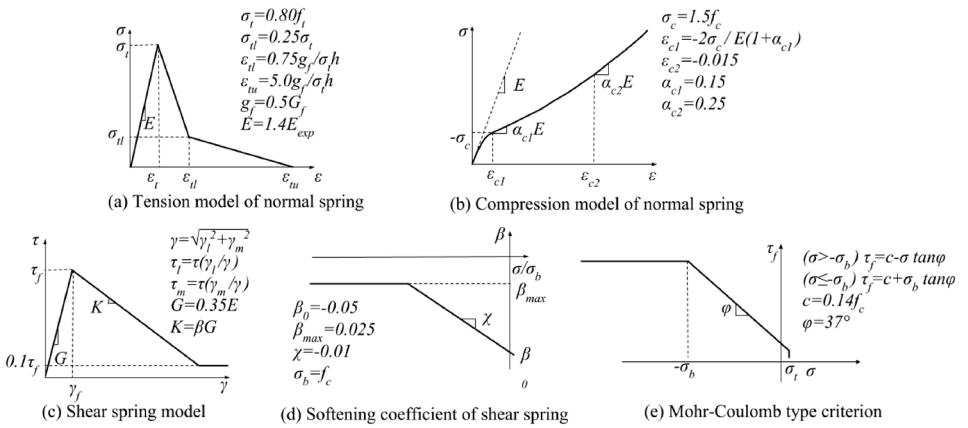


**Fig. 3.** Concrete material model.

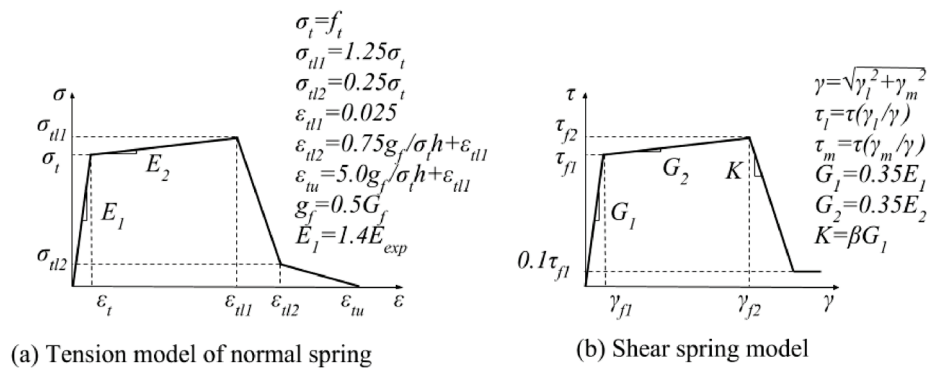


**Fig. 4.** PVA-ECC material model.

The shear stress-strain relation is defined as a combination of the stresses and strains of two shear springs ($\gamma_l$, $\gamma_m$), where *l* and *m* denote two perpendicular directions. The shear stress increases elastically with the slope of the shear modulus, *G*, up to the shear strength, $\tau_f$. Then, the softening behavior is assumed (Figure 3c)). The slope of softening, *K*, depends on the normal spring stresses through the softening ratio, $\beta$, that increases up to the maximum value with increase of the tensile stresses (Figure 3d)) [8, 9]. The shear behavior is defined by the following formulas

$$\tau = \begin{cases} G\gamma & \gamma < \gamma_f \\ \max\left(\tau_f + K(\gamma-\gamma_f), 0.1\tau_f\right) & \gamma \ge \gamma_f \end{cases} \quad \text{and} \quad \beta = \min\left(\beta_0 + \chi(\sigma/\sigma_b), \beta_{\max}\right) \tag{2}$$

The Mohr-Coulomb type criterion is assumed as the shear spring failure criterion (Figure 3e)) [8, 9]. The decrease of the shear stress with the increase of the crack width is taken into consideration as follows [8, 9],

$$\tau = \begin{cases} \beta_{cr} G\gamma & \gamma < \gamma_{ft} \\ \beta_{cr} \max\left(\tau_{ft} + K\left(\gamma_{\max} - \gamma_{ft}\right), 0.1\tau_f\right) & \gamma \geq \gamma_{ft} \end{cases} \quad (3)$$

where $\beta_{cr} = \frac{\varepsilon_t}{\varepsilon} \exp\left\{\frac{k}{\varepsilon_{tu}}\left(\varepsilon - \varepsilon_t\right)\right\}$, $\tau_{ft} = c - \sigma_t \tan\varphi$.

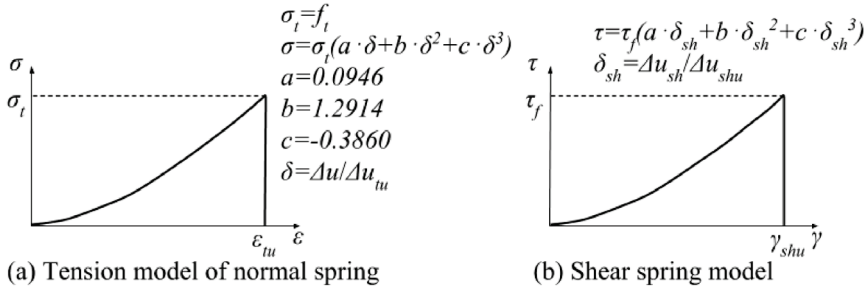


(a) Tension model of normal spring (b) Shear spring model

**Fig. 5.** PVA-ECC-to-concrete bond material model.

## 2.2 PVA-ECC material model

The material model for the PVA-ECC in tension was taken from the experimental investigation of the PVA-ECC with 2% fiber content [10], and is shown in Figure 4a). The normal spring in tension is modeled as linear elastic up to the tensile strength $\sigma_t$ with a linear hardening branch after cracking and a bilinear softening behavior after crack localization. The strain characteristics of the PVA-ECC derived from the fracture energy of concrete with the assumption that PVA-ECC behavior before cracking and after crack localization is similar to concrete behavior [10]. Since the compression behavior of the PVA-ECC is close to concrete (see Figure 3 b)) [10], the compression model of the PVA-ECC is assumed to be the same as in the material model for concrete and is given by Eq. 1.

The shear stress-strain diagram is shown in Figure 4b) where the slope of softening $K$ also depends on the normal spring stresses through the softening ratio $\beta$ (see Figure 3d)) and thus is also given by Eqs. 2 and 3. The Mohr-Coulomb type failure criterion is also assumed (see Figure 3e)), where

$$\tau_{f1} = \tau_f \quad \text{and} \quad \tau_{f2} = \begin{cases} c - 0.8\sigma\tan\varphi & \sigma > -\sigma_b \\ c - 1.25\sigma\tan\varphi & \sigma \leq -\sigma_b \end{cases} \quad (4)$$

## 2.3 Bond between concrete and PVA-ECC material model

The trend of the stress-strain curve of the bond is similar to the stress-strain curve of the PVA fibers in tension [11], which means that the bond is provided mostly by the PVA fibers. The tensile bond behavior was presented in previous numerical and experimental study [5], where the tensile stress-strain relation is expressed by a cubic parabola up to the failure without any softening brunch (Figure 5a)), where $\Delta u$ is the relative normal displacement of the spring and $\Delta u_{tu}$ is its ultimate relative normal displacement.

The bond compression strength is accepted as the average of the strengths of the PVA-ECC and concrete. The stress-strain relation is shown in Figure 3b).

The shear behavior is similar to that in tension and is shown in Figure 4b), where $\Delta u_{sh}$ is the relative shear displacement of the spring and $\Delta u_{shu}$ is its ultimate relative shear

displacement. The shear spring model has no softening branch, but the Mohr-Coulomb type failure criterion shown in Figure 3e) is assumed.

## 3 Numerical analysis

A concrete frame corner with and without a PVA-ECC repair layer subjected to the bending moment (Figure 6) is considered in this study. This structural detail is chosen due to concave corner presence, which may produce serious problems because of non-uniform stiffness distribution and restriction of deformation [12]. Numerical analysis is performed in Matlab using non-linear 3D RBSM. The material parameters considered in the analyses were as follows. For concrete: $E_{exp}$ = 35GPa, $f_t$ = 3.5MPa, $f_c$ = 40MPa and $G_f$ = 100N/m. For the PVA-ECC: $E_{exp}$ = 20GPa, $f_t$ = 5MPa, $f_c$ = 50MPa. For bond between concrete and PVA-ECC: $f_t$ = 1.5MPa, $f_c = (f_{c,conc}+f_{c,ECC})/2$ = 45MPa, $\Delta u_{tu}$ = 0.473mm and $\Delta u_{shu}$, = 1mm.

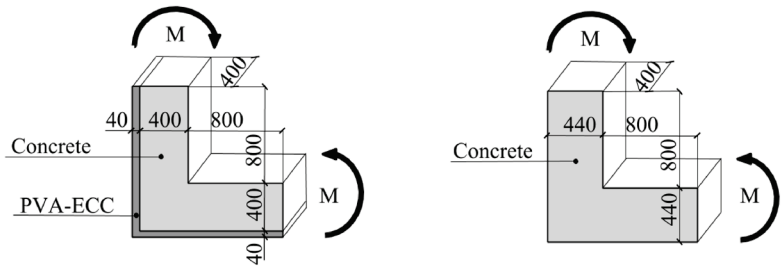


**Fig. 6.** Analyzed frame corner.

The analyzed frame corner was loaded with displacement as shown in Figures 7 and 8. The load was divided into 30 load steps of 8 μm each. Displacement-controlled modified Newton-Raphson method was used as the convergence algorithm. Convergence of the model is attained when the Σ(Reaction of elements in the model)$^2$ becomes less than $10^{-6}$. When the model did not converge at a given maximum iterations (maximum number of iterations = 400), the analysis proceeded to the next step [13].

## 4 Results and discussion

The crack patterns obtained from the numerical analyses are shown in Figures 7 and 8. The results show that the sample destruction starts in concrete part. PVA-ECC layer affects weakly the crack pattern and cracks width in concrete, but it provides thinner cracks on the surface of concrete frame corner, which slows the chemical particles transfer, which is verified by experimental investigation [14].

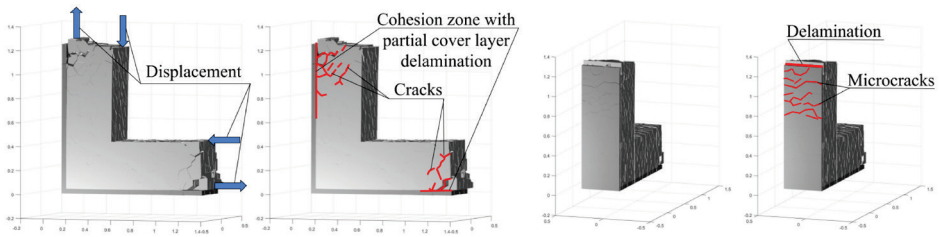


**Fig. 7.** Crack pattern in frame corner with PVA-ECC overlay. (magnification=150).

The PVA-ECC layer is partially delaminated and creates a cohesion zone between the two materials (Figure 7) because of high ductility and lower strength of bond in tension, so

the damaged concrete parts are slightly pulled out of PVA-ECC layer, while the PVA-ECC layer is not broken due its high ductility and strain hardening in tension.

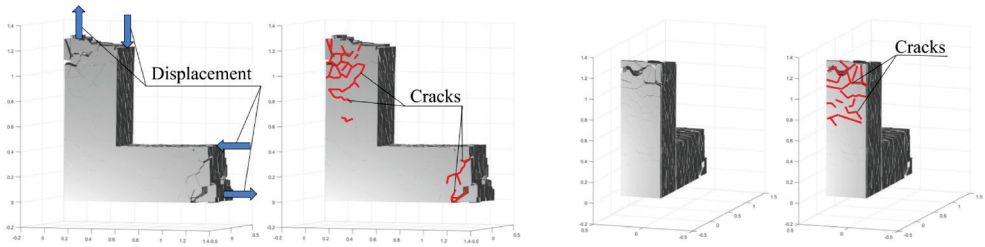


**Fig. 8.** Crack pattern in frame corner without PVA-ECC overlay. (magnification=150).

## 5 Conclusions

According to the results of the numerical analyses, the PVA-ECC overlay helps to reduce crack width on a surface of the modelled structural detail so that the rate of penetration of aggressive chemicals in concrete can be reduced, which is in accordance with the experimental investigation reported in [14]. The PVA-ECC provided a relatively strong bond with concrete with occurrence of insignificant delamination. Thus, the PVA-ECC becomes a suitable material for concrete cover repairs.

The Rigid-Body-Spring Model (RBSM) method with random Voronoi tessellation proved suitable for analyses of repair layers, since it is able to determine the crack pattern, crack width and possible cover layer delamination, while using simple material model.

This work was financially supported by the Czech Science Foundation, project 15-11753S, and the Czech Technical University in Prague (CTU), project SGS17/048/OHK1/1T/11, which are gratefully acknowledged.

## References

1. J. Ślusarek, A. Kostrzanowska, ACEE. **1**, 85-92 (2010)
2. M. Li, V.C. Li, Restoration of Buildings and Monuments. **12(2)**, 143-160 (2006)
3. V.C. Li, Concrete: material science to application. **SP 206-23**, 373-400 (2002)
4. V.C. Li, S. Wang, C. Wu, ACI Mater. J. **98(6)**, 483-492 (2001)
5. G. Fischer, V.C. Li, ACI Struct. J. **99(1)**, 104-111 (2002)
6. T. Kawai, Nucl. Eng. Des. **48**, 207-229 (1978)
7. J.E. Bolander, S. Saito, Eng. Fract. Mech. **61**, 569-591 (1998)
8. Y. Yamamoto, H. Nalamura, I. Kuroda, N. Furuya, Eur. J. of Environ. Civ. En. **18,** 780-792 (2014)
9. K. Nagai, Y. Sato, T. Ueda, J. Adv. Concr. Technol., **3**, 385-402 (2005)
10. I. Paegle, G. Fischer, Proc. Of the Int. Conf. "Innovative Materials, Structures and Technologies", 122-128 (2013)
11. M.S. Magalhaes, R.D. Toledo Filho, E.M. Rego Fairbairn, Matéria (Rio de Janeiro), **18**, 1587-1595 (2013)
12. Y. Yang, Y. Wang, F. Fu, J. Liu, Thin Wall Struct. **95**, 674-388 (2015)
13. Y. Ishikawa, H. Nakamura, T. Tanabe, Proc. of JCI meeting, **25**, 467-472 (2003) (In Japanese)
14. M. Sahmaran, V.C. Li, Cement Concrete Comp., **33**, 72-81 (2008)